PAPER

Check for updates

cis-Thioindigo (TI) – a new ligand with accessible radical anion and dianion states. Strong magnetic coupling in the {[TI-(μ2-O),(μ-O)]Cp*Cr}2 dimers†

Dmitri V. Konarev, [*a] Salavat S. Khasanov,[b] Alexander F. Shestakov,[a] Alexey M. Fatalov,[a,c] Mikhail S. Batov, [a,c] Akihiro Otsuka,[d,e] Hideki Yamochi,[d,e] Hiroshi Kitagawa [d] and Rimma N. Lyubovskaya[a]

Reaction of decamethylchromocene (Cp*$_2$Cr) with thioindigo (TI) yields a coordination complex {[TI-(μ$_2$-O), (μ-O)]Cp*Cr}$_2$·C$_6$H$_{14}$ (**1**) in which one Cp* ligand in Cp*$_2$Cr is substituted by TI. TI adopts *cis*-conformation in **1** allowing the coordination of both carbonyl groups to chromium. Additionally, one oxygen atom of TI becomes a μ$_2$-bridge for two chromium atoms to form {[TI-(μ$_2$-O), (μ-O)]Cp*Cr}$_2$ dimers with a Cr···Cr distance of 3.12 Å. According to magnetic data, diamagnetic TI^{2-} dianions and two Cr^{3+} atoms with a high S = 3/2 spin state are present in a dimer allowing strong antiferromagnetic coupling between two Cr^{3+} spins with an exchange interaction of −35.4 K and the decrease of molar magnetic susceptibility below 140 K. Paramagnetic TI$^{•-}$ radical anions with the S = 1/2 spin state have also been obtained and studied in crystalline {cryptand[2,2,2](Na$^+$)}(TI$^{•-}$) (**2**) salt showing that both radical anion and dianion states are accessible for TI.

Introduction

Indigo and its derivatives are known as organic dyes produced on a ton scale.[1] Indigo is also used as an electronic material and component in rechargeable batteries.[2] Indigo forms coordination complexes with transition metals. They are obtained for deprotonated indigo in monoanionic (indigoH$^-$) and dianionic (indigo^{2-}) states. In all these complexes, indigo adopts a *trans*-conformation coordinating to the metal center by both carbonyl oxygen and nitrogen atoms.[3] Recently, we found that indigo substitute the pentamethylcyclopentadienyl (Cp*) ligand of decamethylchromocene (Cp*$_2$Cr) forming a mononuclear (indigo-*O*,*O*)(Cp*Cr^{II}Cl) complex in which indigo adopts *cis*-conformation allowing the coordination of both carbonyl oxygen atoms to chromium.[4]

Thioindigo (TI) is also a well-known dye[5] related to indigo but containing sulfur atoms instead of the N–H groups (Fig. 1). TI shows intense absorption in the visible range and a color in solution and solid state. Potentially it is also able to form stable complexes with transition metals by employing the carbonyl groups. However, in contrast to indigo, no coordination complexes of TI are known. Any information about the structure and properties of the TI radical anions or dianions in solid state is also absent.

In this work we studied the reaction of TI with decamethylchromocene (Cp*$_2$Cr) and obtained the first transition metal complex of thioindigo {[TI-(μ$_2$-O), (μ-O)]Cp*Cr}$_2$·C$_6$H$_{14}$ (**1**). We also synthesized {cryptand[2,2,2](Na$^+$)}(TI$^{•-}$) (**2**) containing the TI$^{•-}$ radical anions to understand the charged state of TI in **1**.

^{a}*Institute of Problems of Chemical Physics RAS, Chernogolovka, 142432 Russia.*
E-mail: konarev3@yandex.ru
^{b}*Institute of Solid State Physics RAS, Chernogolovka, 142432 Russia*
^{c}*Lomonosov Moscow State University, Leninskie Gory, Moscow, 119991 Russia*
^{d}*Division of Chemistry, Graduate School of Science, Kyoto University, Sakyo-ku, Kyoto 606-8502, Japan*
^{e}*Research Center for Low Temperature and Materials Sciences, Kyoto University, Sakyo-ku, Kyoto 606-8501, Japan*
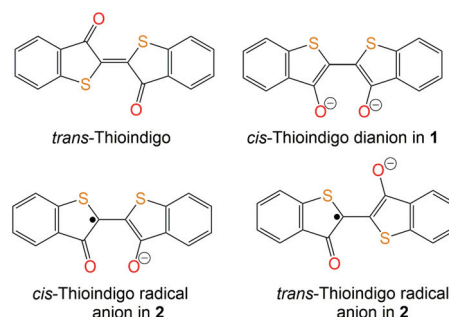
Fig. 1 Schematic presentation of the molecular structures of pristine *trans*-TI, *cis*-TI^{2-} dianion in **1** and *cis*- and *trans*-forms of the TI$^{•-}$ radical anion in **2**.

Crystal structures, and optical and magnetic properties of **1** and **2** are discussed and a possible mechanism for the formation of **1** is presented.

Results and discussion

Synthesis

Thioindigo immediately gave a red-violet solution when combined with Cp*$_2$Cr, and the color changed to red-brown after one hour. The structure of **1** was determined from X-ray diffraction on single crystals. Several crystals tested from the synthesis showed them to belong to one phase only.

Similar to indigo, TI also substitutes the Cp* ligand at the chromium atom of Cp*$_2$Cr. However, indigo and TI form different complexes with Cp*Cr and have different charges in these complexes. The different features of TI and indigo are understood mainly by the variation of their redox properties and the magnitude of energy difference between the *cis*- and *trans*-isomers. TI shows essentially stronger acceptor properties with first and second reduction potentials $E_{red} = -0.305$ and -0.97 V *vs.* Ag/AgClO$_4$ in 0.1 M solution of TBAClO$_4$ in DMF or -0.01 and -0.67 V *vs.* SCE, respectively.[6] The first reduction potential of indigo is essentially more negative (-0.75 V *vs.* Ag/AgCl or -0.795 and *vs.* SCE).[7] As a result, deeper reduction of TI is possible in the complexes in comparison with indigo. Unlike indigo, TI has a smaller energy difference between ground state *trans*- and *cis*-forms. The calculated values are 11.6 and 13.4 kcal mol^{-1} for neutral and negatively charged TI molecules, respectively. The corresponding values for indigo are 16.7 and 20.6 kcal mol^{-1}, respectively. The reason is the absence of short H···H contacts for *cis*-TI.

Since Cp*$_2$Cr is a strong donor with the first oxidation potential of -1.04 V *vs.* SCE,[8] it can reduce TI to form a rather stable outer-sphere charge transfer complex (Cp*$_2$Cr$^+$)(TI$^{•-}$).

With the aid of quantum chemical calculations, the reaction mechanism to produce **1** is inferred as follows. The formation of (Cp*$_2$Cr$^+$)(TI$^{•-}$) is accompanied by an energy decrease of 8.5 kcal mol^{-1} (Fig. 2). The color change of reaction solution mentioned above is most probably caused by the formation of a coordination complex. This complex can form *via* an intermediate (*trans*-TI-*O*)Cp*$_2$Cr complex with the formation of an isomeric (*cis*-TI-*O*,*O*)Cp*$_2$Cr complex accompanied by the subsequent η^5–η^1 shift of the Cp* ring (see the ESI† for a more detailed mechanism). This leads to a slight increase in energy by 2.5 kcal mol^{-1} (Fig. 2). Therefore, the equilibrium concentration of the (*cis*-TI-*O*,*O*)Cp*$_2$Cr complex is expected to be sufficient for bimolecular reaction of transformation of this complex into binuclear complex **1** with the subtraction of two Cp* rings in the form of the (Cp*)$_2$ dimer. This process proceeds with a noticeable energy gain of 33.6 kcal mol^{-1} explaining the formation of **1**.

In previous work[4] we showed that the complex (indigo-*O*,*O*)(Cp*Cr^{II}Cl) is formed only in the presence of chloride anions the source of which is the chloro(1,5-cyclooctadiene)rhodium(I) dimer, {Rh^I(cod)Cl}$_2$. The {Rh^I(cod)Cl}$_2$ can accept also the Cp* ligand leaving from Cp*$_2$Cr. Without the addition of the {Rh^I(cod)Cl}$_2$ the coordination complex of indigo is not formed.[4] The TI reaction is realized without {Rh^I(cod)Cl}$_2$. Since TI is negatively charged in **1**, it is possible that chloride anions are not needed to compensate for the positive charge of chromium atoms. The absence of a chloride substituent at the chromium atom in **1** opens a position for coordination of the third oxygen atom of TI which becomes a μ_2-bridge bonding two [TI-*O*,*O*]Cp*Cr units into a dimer (Fig. 3a). For the (*cis*-indigo-*O*,*O*)Cp*$_2$Cr complex, a similar process accompanied by the formation of an {[indigo-(μ_2-*O*),(μ-*O*)]Cp*Cr}$_2$ dimer, which is an analog of complex **1**, has also a significant energy gain. The absence of such a product is caused by the thermodynamically unfavorable formation of an
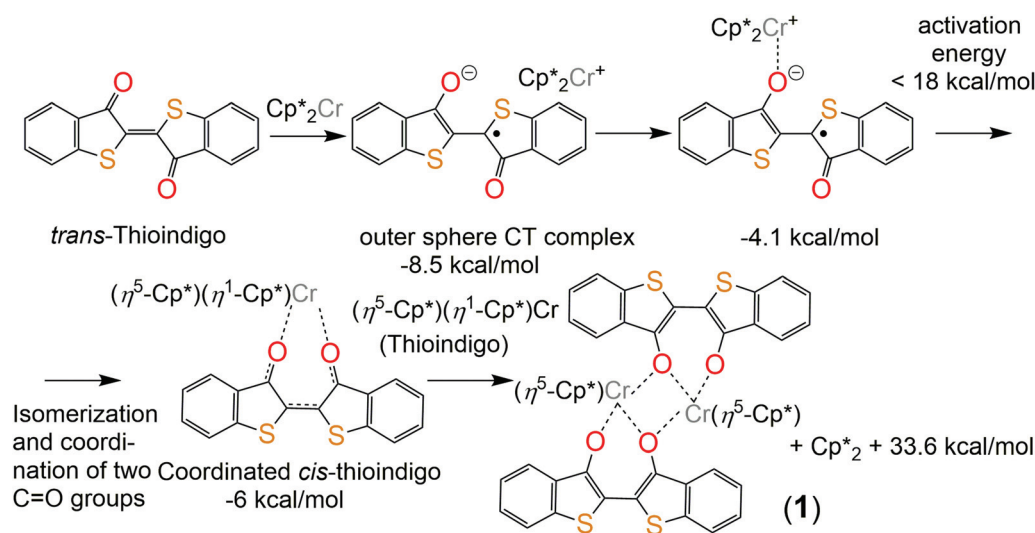
Fig. 2 Scheme of the possible reaction of TI with decamethylchromocene. All energies below the structures are given relatively to one level – free Cp*$_2$Cr and *trans*-thioindigo.
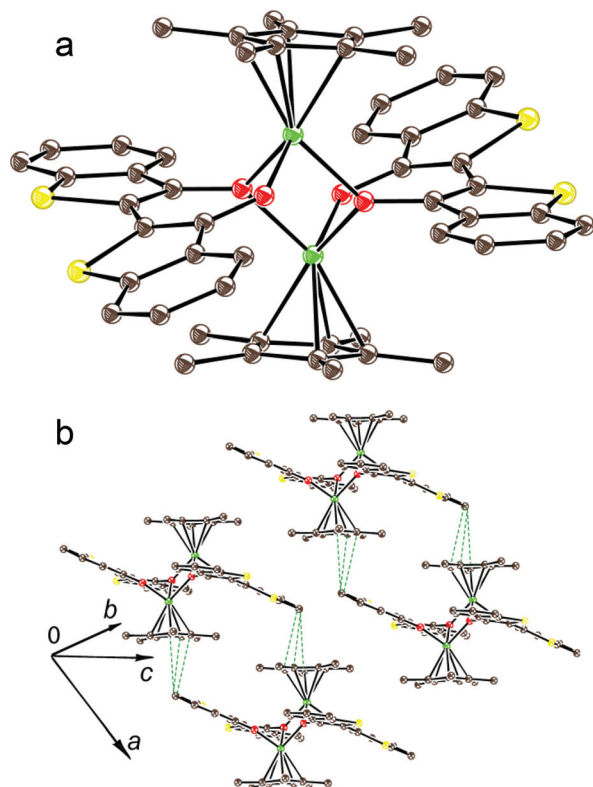
Fig. 3 View on the {[TI-(μ_2-O),(μ-O)]Cp*Cr}$_2$ dimers in **1** (carbon is brown, chromium is green, oxygen is red and sulfur is yellow) (a); packing of the dimers in the crystal structure of **1** (b).

intermediate (*cis*-indigo-O,O)Cp*$_2$Cr complex. As a result, its effective concentration is low, and only bimolecular processes of substitution of the Cp* ligand by the chloride anion are possible in the presence of {Rh^I(cod)Cl}$_2$ which is present in high concentration.

Crystal structures

The crystal structure of **1** was studied at 200 K.‡ The Cp* ligand is disordered between two orientations related by the rotation of this ligand by 15.84°. Each chromium atom coordinates the Cp* ligand by η^5-type (Fig. 3a) with average Cr–C (Cp*) bonds of 2.230(2) Å. These distances are noticeably longer in comparison with that of pristine Cp*$_2$Cr (2.152(4) Å)[9]

and are closer to those in the (Cp*$_2$Cr)$^+$ cations (the average Cr–C(Cp*) bond length is 2.176(3)–2.198(3) Å).[10] Moreover, two oxygen atoms of each TI coordinate to each chromium atom (Fig. 3a). Two oxygen atoms belong to one TI and have short Cr–O distances of 1.922(1) and 1.989(1) Å. The third oxygen atom belongs to the opposite TI, and the Cr–O distance is 2.004(1) Å. Since one of the two oxygen atoms for each TI becomes a μ_2-bridge for two chromium atoms, such coordination provides the formation of dimers in which chromium atoms are separated only by one oxygen atom with a short Cr···Cr distance of only 3.126(2) Å. The Cp* planes in the dimers are nearly parallel and are separated by the 6.334 Å distance in **1**.

The geometry of TI in **1** is listed in Table 1. The distinct modulation of bond lengths is observed in TI at the formation of **1**. The central C=C bond and the C=O bonds elongate and become close to the single C–C and C–O bonds, whereas the C(O)–C(C) bonds are shortened to the length of the double C=C bond. Such bond length variation indicates the dianion state of TI in **1** and agrees well with the molecular formula proposed for the indigo and TI dianions (Fig. 1). To distinguish the geometry of the TI dianion from that of the radical anion we also synthesized crystalline salt {cryptand[2,2,2](Na$^+$)}(TI$^{•-}$) (**2**).‡ Unfortunately, disorder appears in the structure of **2** due to the presence of both *trans*- and *cis*-conformations for two independent TI with orientational disorder of the conformations. One of the independent TI molecules has the occupancy for the disordered S and CO groups of 0.607/0.393 and 0.861/0.139. These values of occupancy lead to 0.254 for *trans*-conformation, at least, and 0.468 for *cis*-conformation, at least (Fig. S13†). The second independent TI molecule has higher scattering of *trans*/*cis* ratio, again the lowest possible occupancies are 0.114 and 0.124 for the *trans*- and *cis*-conformations, respectively. We discuss the molecular structure of the first TI$^{•-}$ in **2** (Table 1). The central C=C bond in TI$^{•-}$ has an intermediate length between those for neutral and dianion TI. At the same time both C=O bonds are elongated but both C(O)–C(=) bonds are shortened in TI$^{•-}$ in comparison with *trans*-TI (Table 1). Such geometry change agrees with the delocalized feature of one negative charge over the two oxygen atoms of TI$^{•-}$, one of the canonical structures of which is shown in Fig. 1. DFT calculations of the molecular geometry of TI$^{•-}$ in *cis*- and *trans*-conformations (Fig. S1†) also support delocalization of negative charge over two oxygen atoms of TI$^{•-}$ (Table 1). Pristine *trans*-TI adopts a planar conformation around the central C=C bond.[11,12] An increased length of the C=C bond in the radical anion and dianion states reduces the double bond nature of this bond. As a result, the dihedral angle between two planar C$_6$H$_4$SC(=O)C fragments increases to 6–7° for the radical anion in **2** and up to 19.7° for the dianion in **1** which nearly corresponds to the central C–C single bond. The S–C bonds are not so sensitive to the charged state of TI (Table 1).

The packing mode of the {[TI-(μ_2-O),(μ-O)]Cp*Cr}$_2$ dimers in **1** is shown in Fig. 3b. There are short S, C(TI)–C(Cp*) contacts in the 3.20–3.46 Å range between TI and Cp* ligands but

Table 1 Bond length (Å) and dihedral angle of TI in different charged states

Compound	Central C=C bond	Average C=O bond	Average C(O)–C(=) bond	Average S–C(=) bond	Average S–C(Phen) bond	Dihedral angle[b] (°)
Tetrachlorothioindigo[11]						
trans-Conformation (0.65)	1.345(2)	1.200(2)	1.447(2)	1.783(3)	1.766(3)	0.01
cis-Conformation (0.35)	1.345(2)	1.204(2)	1.452(2)	1.799(3)	1.783(3)	1.01
trans-TI[12]	1.34(3)	1.21(3)	1.54(3)	1.78(3)	1.74(3)	0
TI[·−] radical anion in **2**[a]						
trans-Conformation	1.411(8)	1.270(18)	1.356(15)	1.860(9)	1.726(8)	6.40
		1.34(3)	1.331(11)			
cis-Conformation	1.411(8)	1.330(8)	1.305(12)	1.803(5)	1.730(6)	7.46
		1.377(12)	1.331(8)			
Calculated *cis*-TI[·−] radical anion	1.404	1.242	1.474	1.781	1.753	—
Calculated *trans*-TI[·−] radical anion	1.388	1.256	1.454	1.768	1.765	—
cis-TI[2−] dianion in **1**	1.445(2)	1.332(2)	1.377(2)	1.762(2)	1.731(2)	19.7

[a] Geometry of the more ordered TI[·−] radical anion among the two crystallographically unique ones is considered. [b] Dihedral angle around the central C=C bond between two planes defined by SCC(=O) atoms.

the TI and Cp* fragments are arranged nonparallel to each other. Therefore, intermolecular π–π interactions between the dimers are weak.

Optical properties

Pristine TI has two bands in the UV-visible spectrum with maxima at 281 and 547 nm (Fig. 4a). Reduction of TI to the radical anion in **2** provides the appearance of new bands in the 500–760 nm range and a noticeable blue shift of the most intense band at 547 to 440 nm (Fig. 4b). At the same time, the band at 281 nm in the UV range retains its position in the spectrum of **2** at 292 nm (Fig. 4b). Thus, reduction essentially increases the energy of the π–π* transitions[13] in TI. The series

Fig. 4 UV-visible-NIR spectra of neutral TI (a); salt {cryptand[2,2,2](Na^{+})}(TI[·−]) (**2**) with the TI[·−] radical anions (b) and coordination complex {TI-(μ2-O),(μ-O)Cp*Cr}2 (**1**) with the TI[2−] dianions (c). Spectra are recorded as KBr pellets prepared under anaerobic conditions. The inset shows the calculated spectrum for complex **2**.

of bands at 576, 700 and 736 nm can be attributed to TI[·−] since these bands are absent in the spectrum of neutral TI (Fig. 4a). The appearance of several bands can be explained by the presence of different conformations of the molecule which can have different positions of these bands. The formation of TI[2−] dianions in **1** is accompanied by an even stronger blue shift of the intense band in the visible range up to 426 nm (Fig. 4c), whereas the band in the UV-range is positioned at 307 nm. Several bands of TI[·−] observed in the spectrum of **2** at 500–760 nm are not manifested in the spectrum of **1** (Fig. 4c). Instead of these bands a broad and relatively weak band is manifested in the spectrum of **1** with maximum at 594 nm. According to calculations this broad band is attributed to the transitions from HOMOs localized on TI ligands to LUMOs localized on metal centers and interligand transitions. Thus, TI shows definite spectra in neutral, radical anion and dianion states which allow the charged state of TI to be defined.

IR spectra of TI are shown in Fig. S7–S9† and listed in Table S1.† Reduction of TI affects the C=O stretching mode. Neutral TI manifests two intense bands at 1588 and 1657 cm^{−1} attributed to vibrations of the double C=O bond (Fig. S7†). Since according to the calculations *trans*- and *cis*-TI should have the position of these bands in the IR-spectra at 1584, 1655 cm^{−1} and 1582, 1713 cm^{−1}, respectively, we can conclude that mainly *trans*-TI is present in the starting compound. Reduction decreases strongly the intensity of these bands in the spectrum of **2** (only band at 1586 cm^{−1} is retained) and a new band appears at 1503 cm^{−1} (Fig. S8†). The bands in the 1550–1600 cm^{−1} region are very weak in the spectrum of **1** indicating disappearance of double C=O bonds in the dianion state of TI (Fig. S8†). Calculations show that bands of the C–O vibrations together with the contribution from the valent C–C vibrations are manifested mainly at 1464, 1409, 1369 and 1350 cm^{−1} (see ESI†).
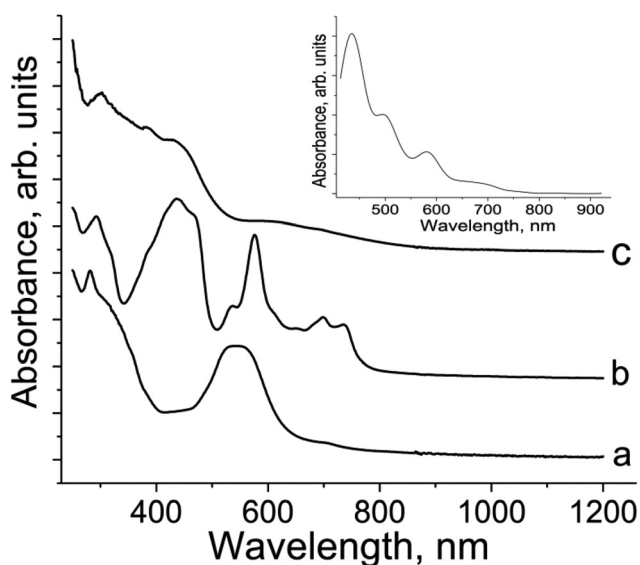
Magnetic properties

Magnetic properties of **1** were studied by EPR and SQUID techniques. Magnetic behavior is described by two contributions:

the main contribution from high-spin Cr^{III} atoms with the $S = 3/2$ spin state and the contribution from the Curie impurities which originates from about 1.5% of $S = 3/2$ spins per dimer (Fig. 5a). These impurities show pure paramagnetic behavior with Weiss temperature close to 0 and are manifested mainly below 15 K. Magnetic behavior of **1** indicates strong antiferro-

Fig. 5 Temperature dependencies of: (a) molar magnetic susceptibility of polycrystalline **1** fitted by two contributions from paramagnetic Curie impurities (red curve) and antiferromagnetically coupled Cr^{III} atoms (blue curve); (b) the $\chi_M T$ value; (c) reciprocal molar magnetic susceptibility of **1** (fitting of the high-temperature data (160–300 K) by the Curie–Weiss law with Weiss temperature of −250 K is shown by the red line); (d) modelling of the data by the general exchange Hamilton for the pairs of Cr^{III}.

magnetic coupling between spins which results in the decrease of magnetic susceptibility of **1** below 140 K and gives the singlet ground state at the lowest temperatures due to an anti-parallel arrangement of the Cr^{III} spins within the dimers. The $\chi_M T$ value of **1** is equal to 3.14 emu K mol^{-1} at 300 K (Fig. 5b). This corresponds to an effective magnetic moment of $5.03\mu_B$ (Fig. S19b†) which does not attain the theoretical value of $5.48\mu_B$ calculated for the system of two noninteracting $S = 3/2$ spins due to their strong antiferromagnetic coupling. As a result, the $\chi_M T$ value (Fig. 5b) or effective magnetic moment (Fig. S19b†) of **1** decreases with temperature below 300 K. Weiss temperature of −250 K estimated in the 160–300 K range also confirms strong antiferromagnetic coupling between the Cr^{III} spins (Fig. 5c).

The magnetic properties of the Cr(III) dimers[14] were modeled by including biquadratic exchange interactions (j) according to the general exchange Hamiltonian $H = -2J\mathbf{S}_1 \cdot \mathbf{S}_2 - j(\mathbf{S}_1 \cdot \mathbf{S}_2)^2$, where j is the biquadratic exchange constant.[15] This leads to the following expression:

$$\chi_M = \frac{2Ng^2\mu_B{}^2}{kT}$$
$$\times \left\{ \frac{e^{(2j-6.5j)/kT} + 5e^{(6j-13.5j)/kT} + 14e^{(12j-9j)/kT}}{1 + 3e^{(2j-6.5j)/kT} + 5e^{(6j-13.5j)/kT} + 7e^{(12j-9j)/kT}} \right\}$$

Using this model with $J = -24.6$ cm^{-1} or −35.4 K, $j = 1.5$ cm^{-1}, $g = 1.98$ the experimental data (Fig. 5d, black squares) can be fitted well (Fig. 5d, red curve). The g-factor nearly 1.98 is typical of Cr(III) complexes.[15] The value of magnetic exchange interaction of $J = -35.4$ K reflects very effective magnetic coupling between two Cr(III) atoms through two oxygen bridges of TI^{2-}. The exchange coupling can be estimated based on the Weiss constant. In the mean field approximation the Weiss constant relates to the exchange coupling by: $\Theta = 2zJS(S + 1)/3k$, where z = number of the nearest neighbors ($z = 1$ for a dimer). Using $\Theta = -250$ K an initial estimate gives $J/k = -33$ K based on $S = 3/2$. This value is in good agreement with that derived from the Cr-dimer model. To estimate the contribution from the TI ligand we studied magnetic behavior of **2**. This salt contains the $TI^{\bullet-}$ radical anions with the $S = 1/2$ spin state providing an effective magnetic moment of $1.71\mu_B$ at 300 K (Fig. S14†) characteristic of one noninteracting $S = 1/2$ spin ($1.73\mu_B$). The salt shows nearly paramagnetic behavior with a Weiss temperature of −1 K (Fig. S15†) due to the absence of π–π interactions between $TI^{\bullet-}$ (Fig. S12†). Salt **2** manifests an intense EPR signal with a nearly temperature independent g-factor of 2.0051 and the linewidth of 0.6–0.7 mT (Fig. S16–S18†). Observation of this signal allows one to determine unambiguously the presence of $TI^{\bullet-}$ in the compound. Magnetic moment of **1** indicates the absence of contribution from $TI^{\bullet-}$ since higher magnetic moment is expected in this case. EPR spectra of polycrystalline **1** at 140, 59 and 6.5 K are shown in Fig. S20–S22.† The complex pattern at all these temperatures most likely arises from zero field splitting. We used the parameters J and j of spin Hamiltonian, which allows the magnetic susceptibility of **1** to be described well,
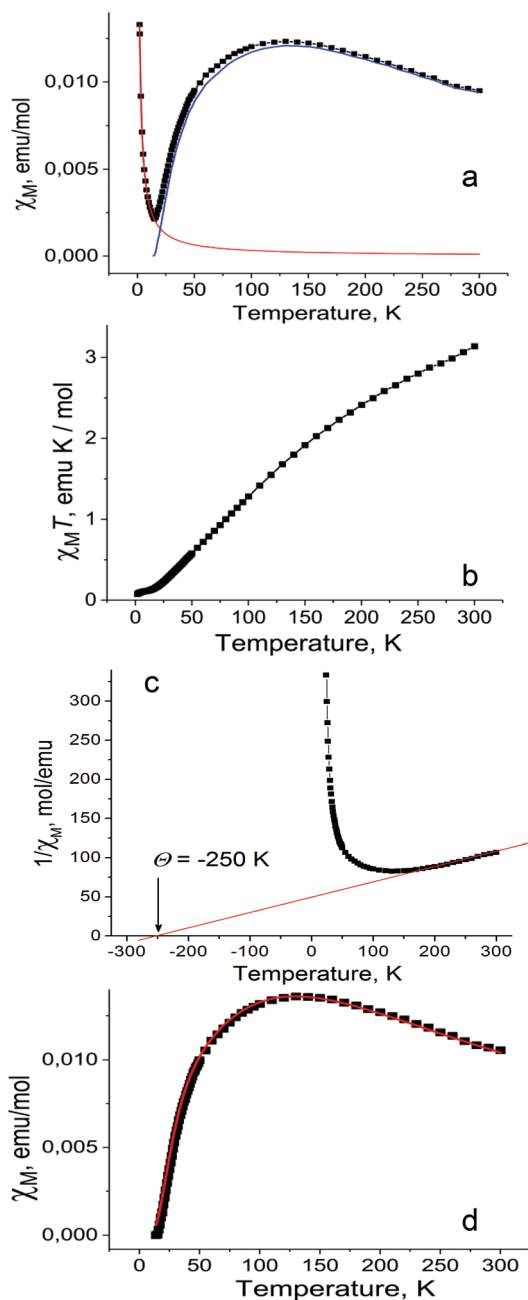
to calculate the temperature dependence of the population of different spin states $S = 1, 2$ and 3 of the dimer. The population of all magnetic states is very low at 6.5 K, and the EPR spectrum is mainly defined by the Curie impurities (Fig. S22†). At the same time at 59 K populations of these states became 0.40, 0.05 and 0.002, respectively. Therefore, the spectrum of a nearly pure triplet state is observed at 59 K (Fig. S21†). The spectrum at 140 K is similar to that at 59 K at high and low magnetic fields but additional signals appear at 320–420 mT (Fig. S20†). Estimation gives the following population of the $S = 1, 2$ and 3 states, namely, 0.43, 0.23 and 0.08, respectively. The population of quintet states increases at 140 K and the admixture of the septet state appears. Therefore, additional signals at intermediate fields (320–420 mT) can most probably be attributed to the quintet state. The absence of narrow signals from $TI^{•-}$ in the EPR spectrum of **1** supports the formation of diamagnetic and EPR silent TI^{2-} dianions. All these data indicate the ionic formula of **1** as $\{[TI^{2-}\text{-}(\mu_2\text{-}O),(\mu\text{-}O)](Cp^{*-})(Cr^{III})\}_2 \cdot C_6H_{14}$ and that agrees with the redox potential of TI. In contrast, in the case of indigo no charge transfer was found from chromium(II) to indigo in the ground state of the (indigo-O,O)^0[(Cp^{*-})Cr^{II}(Cl$^-$)] complex.[4]

Experimental

Materials

Thioindigo and cryptand[2,2,2] (>98%) were purchased from TCI. Decamethylchromocene (Cp$^*_2$Cr, >95%) and chloro(1,5-cyclooctadiene)rhodium dimer ({Rh^I(cod)Cl}$_2$, 98%) were purchased from Strem. Sodium fluorenone ketyl was obtained as described.[16] o-Dichlorobenzene (C$_6$H$_4$Cl$_2$) was distilled over CaH$_2$ under reduced pressure; n-hexane was distilled over Na/benzophenone. All operations on the synthesis of **1** and **2** and their storage were carried out in a MBraun 150B-G glovebox with a controlled atmosphere in which water and oxygen contents are less than 1 ppm. The solvents were degassed and stored in the glovebox. KBr pellets for IR- and UV-visible-NIR measurements were prepared in the glovebox. Polycrystalline samples of **1** and **2** were placed in 2 mm quartz tubes under anaerobic conditions for EPR and SQUID measurements and sealed under 10^{-5} Torr pressure.

General

UV-visible-NIR spectra were recorded in KBr pellets with a PerkinElmer Lambda 1050 spectrometer in the 250–2500 nm range. FT-IR spectra (400–7800 cm^{-1}) were recorded in KBr pellets with a PerkinElmer Spectrum 400 spectrometer. EPR spectra were recorded for polycrystalline samples of **1** and **2** with a JEOL JES-TE 200 X-band ESR spectrometer equipped with a JEOL ES-CT470 cryostat working between room and liquid helium temperatures. A Quantum Design MPMS-XL SQUID magnetometer was used to measure static magnetic susceptibility of **1** and **2** at 100 mT magnetic field under cooling and heating conditions in the 300–1.9 K range. A sample holder contribution and core temperature independent

diamagnetic susceptibility (χ_d) were subtracted from the experimental values. The χ_d values were estimated by the extrapolation of the data in the high-temperature range by fitting the data with the following expression: $\chi_M = C/(T - \Theta) + \chi_d$, where C is Curie constant and Θ is Weiss temperature. Effective magnetic moment (μ_{eff}) was calculated with the following formula: $\mu_{eff} = (8 \cdot \chi_M \cdot T)^{1/2}$.

Synthesis

The crystals of $\{[TI\text{-}(\mu_2\text{-}O), (\mu\text{-}O)]Cp^*Cr\}_2 \cdot C_6H_{14}$ (**1**) were obtained by the following procedure. 12.5 mg of thioindigo (0.042 mmol) was reduced by slight excess of Cp$^*_2$Cr (15 mg, 0.056 mmol) in 16 mL of o-dichlorobenzene. At the beginning, thioindigo completely dissolved in 10 minutes to form a red-violet solution. Intense stirring at 80 °C for 8 hours resulted in the colour change from red-violet to red-brown. The solution was cooled down to room temperature and filtered into a 50 mL glass tube of 1.8 cm diameter with a ground glass plug, and 30 mL of n-hexane was layered over the solution. After slow mixing of two solvents for 1 month the crystals were precipitated on the walls of the tube. Then the solvent was decanted from the crystals and they were washed with n-hexane to yield black parallelepipeds up to 0.6 × 0.3 × 0.3 mm^3 in size in 67% yield. Composition of the crystals was determined from X-ray diffraction analysis on single crystals. We tested several crystals from the synthesis and all of them showed the same unit cell parameters. Therefore, they belonged to one crystal phase. The crystals of $\{[TI\text{-}(\mu_2\text{-}O), (\mu\text{-}O)]Cp^*Cr\}_2 \cdot C_6H_{14}$ (**1**) could also be obtained in the presence of 14 mg of {Rh^I(cod)Cl}$_2$ (0.028 mmol). Obtained black parallelepipeds had the same unit cell parameters showing that a complex of $\{[TI\text{-}(\mu_2\text{-}O), (\mu\text{-}O)]Cp^*Cr\}_2 \cdot C_6H_{14}$ composition also formed in this synthesis.

The crystals of $\{$cryptand[2,2,2](Na$^+$)$\}(TI^{•-})$ (**2**) were obtained by the following procedure. 12.5 mg of thioindigo (0.042 mmol) was reduced by excess of sodium fluorenone ketyl (12 mg, 0.059 mmol) in the presence of one equivalent of cryptand[2,2,2] (16 mg, 0.042 mmol) in 16 mL of o-dichlorobenzene. Intense stirring at 80 °C for 4 hours provided the formation of red-violet solution. The solution was cooled down to room temperature and filtered into the 50 mL glass tube of 1.8 cm diameter with a ground glass plug, and 30 mL of n-hexane was layered over the solution. After slow mixing of two solvents for 1 month the crystals were precipitated on the walls of the tube. Then the solvent was decanted from the crystals and they were washed with n-hexane to yield elongated violet parallelepipeds up to 0.8 × 0.2 × 0.2 mm^3 in size in 74% yield. The composition of the crystals was determined from X-ray diffraction analysis on single crystals. We tested several crystals from the synthesis which showed the same unit cell parameters and belonged to one crystal phase.

Elemental analysis cannot be used to confirm the composition of these compounds due to their air-sensitivity.

X-ray crystal structure determination

The intensity data for the structural analysis were collected on an Oxford diffraction "Gemini-R" CCD diffractometer with

graphite monochromated MoK_α radiation using an Oxford Instrument Cryojet system. Raw data reduction to F^2 was carried out using CrysAlisPro, Oxford Diffraction Ltd. The structures were solved by direct methods and refined by the full-matrix least-squares method against F^2 using SHELX-2013.[17] Non-hydrogen atoms were refined in the anisotropic approximation. Positions of hydrogen atoms were calculated geometrically. There are each two halves of the independent $\{[TI-(\mu_2-O), (\mu-O)]Cp*Cr\}_2$ dimer and C_6H_{14} molecule, respectively, in **1**. The Cp* ligand in the dimer is disordered between two orientations with the 0.634(7)/0.366(7) occupancies. There are two independent cryptand[2,2,2](Na$^+$) cations and the TI$^{\cdot-}$ radical anions in **2**. In one of two independent TI$^{\cdot-}$ the occupation factors for the disordered S and CO groups are 0.607(6)/0.393(6) and 0.861(5)/0.139(5). For second TI$^{\cdot-}$ the occupation factors for the disordered S and CO groups are 0.619(7)/0.381(7) and 0.505(7)/0.495(7). Therefore, totally four orientations are observed for each independent TI$^{\cdot-}$ radical anion. To keep the anisotropic thermal parameters of the disordered fragments within the reasonable limits, the displacement components were restrained using ISOR, SIMU and DELU SHELXL instructions. This resulted in 182 and 436 restraints used for the refinement of the crystal structures of **1** and **2**, respectively.

Quantum chemical calculations

Theoretical calculations were performed using the PBE density functional method[18] and $\Lambda2$ basis[19] of cc-pVTZ quality. All calculations were performed using the PRIRODA program package[20] at Joint Supercomputer Center of the Russian Academy of Sciences. This approach allows geometry of the dimer in **1** to be well reproduced.

Conclusions

In this work we show that TI can transform from the *trans*- to the *cis*-conformation and is able to effectively coordinate to transition metals by oxygen atoms of both carbonyl groups. Moreover, TI is easily reduced to the radical anion and dianion states and it can be considered as a redox active ligand. This ligand forms dianions in $\{[TI^{2-}-(\mu_2-O),(\mu-O)](Cp*^-)(Cr^{III})\}_2 \cdot C_6H_{14}$ (**1**) which are conformationally very flexible due to the formation of a central C–C single bond. In such a state TI forms a binuclear structure in which magnetic exchange interaction between paramagnetic metal atoms can be effectively transferred through the oxygen μ_2-bridges. In contrast to TI, indigo forms only a mononuclear complex under similar conditions as a neutral ligand. This is explained by essentially stronger acceptor properties of TI in comparison with those of indigo. Since TI is a dye and has strong absorption in the visible range, this ligand is suitable for the development of multifunctional coordination complexes which can combine promising optical and magnetic properties. This work is now in progress.

Conflicts of interest

There are no conflicts to declare.

Acknowledgements

Notes and references

1 (a) C. J. Cooksey, *Biotech. Histochem.*, 2007, **82**, 105–125; (b) N. Stasiak, W. Kukuła-Koch and K. Głowniak, *Acta Pol. Pharm.*, 2014, **71**, 215–221.

2 (a) M. Irimia-Vlada, E. D. Głowacki, P. A. Troshin, G. Schwabegger, L. Leonat, D. K. Susarova, O. Krystal, M. Ullah, Y. Kanbur, M. A. Bodea, V. F. Razumov, H. Sitter, S. Bauer and N. S. Sariciftci, *Adv. Mater.*, 2012, **24**, 375–380; (b) E. D. Głowacki, G. Voss and N. S. Sariciftci, *Adv. Mater.*, 2013, **25**, 6783–6800; (c) M. Yao, K. Kuratani, T. Kojima, N. Takeichi, H. Senoh and T. Kiyobayashi, *Sci. Rep.*, 2014, **4**, 3650.

3 (a) W. Beck, C. Schmidt, R. Wienold, M. Steinmann and B. Wagner, *Angew. Chem., Int. Ed.*, 1989, **28**, 1529–1531; (b) A. Lenz, C. Schmidt, A. Lehmann, B. Wagner and W. Beck, *Z. Naturforsch., B: Chem. Sci.*, 1997, **52**, 474–484; (c) J.-Y. Wu, C.-H. Chang, P. Thanasekaran, C.-C. Tsai, T.-W. Tseng, G.-H. Lee, S.-M. Peng and K.-L. Lu, *Dalton Trans.*, 2008, 6110–6112; (d) P. Mondal, M. Chatterjee, A. Paretzki, K. Beyer, W. Kaim and G. K. Lahiri, *Inorg. Chem.*, 2016, **55**, 3105–3116; (e) F.-S. Guo and R. A. Layfield, *Chem. Commun.*, 2017, **53**, 3130–3133.

4 D. V. Konarev, S. S. Khasanov, A. V. Kuzmin, A. F. Shestakov, A. Otsuka, H. Yamochi, G. Saito and R. N. Lyubovskaya, *Dalton Trans.*, 2016, **45**, 17095–17099.

5 (a) G. M. Wyman and W. R. Brode, *J. Am. Chem. Soc.*, 1951, **73**, 1487–1493; (b) D. A. Rogers, J. D. Margerum and G. M. Wyman, *J. Am. Chem. Soc.*, 1957, **79**, 2464–2468; (c) E. Steingruber, Indigo and Indigo Colorants, in *Ullmann's Encyclopedia of Industrial Chemistry*, Wiley-VCH, Weinheim, 2004.

6 L.-S. R. Yeh and A. J. Bard, *J. Electroanal. Chem.*, 1976, **70**, 157–169.

7 A. Roessler, D. Crettenand, O. Dossenbach, W. Marte and P. Rys, *Electrochim. Acta*, 2002, **47**, 1989–1995.

8 J. L. Robbins, N. Edelstein, B. Spencer and J. C. Smart, *J. Am. Chem. Soc.*, 1982, **104**, 1882–1893.

9 J. Blümel, M. Herker, W. Hiller and F. H. Köhler, *Organometallics*, 1996, **15**, 3474–3476.

10 (a) F. Zuo, A. J. Epstein, C. Vazquez, R. S. McLean and J. S. Miller, *J. Mater. Chem.*, 1993, **3**, 215–218;

(*b*) D. V. Konarev, S. S. Khasanov, A. Otsuka and G. Saito, *J. Am. Chem. Soc.*, 2002, **124**, 8520–8521; (*c*) D. V. Konarev, S. S. Khasanov, M. Ishikawa, A. Otsuka, H. Yamochi, G. Saito and R. N. Lyubovskaya, *Dalton Trans.*, 2017, **46**, 3492–3499.

11 K. Fukushima, K. Nakatsu, R. Takahashi, H. Yamamoto, K. Gohda and S. Homma, *J. Phys. Chem. B*, 1998, **102**, 5985–5990.

12 H. von Eller, *Bull. Soc. Chim. Fr.*, 1955, **106**, 1438.

13 W. Lüttke, H. Hermann and M. Klessinger, *Angew. Chem., Int. Ed.*, 1966, **5**, 598–599.

14 (*a*) N. H. Andersen, A. Dossing and A. Molgaard, *Inorg. Chem.*, 2003, **42**, 6050–6055; (*b*) S. J. Cline, J. Glerup, D. J. Hodgson, G. S. Jensen and E. Pedersen, *Inorg. Chem.*, 1981, **20**, 2229–2233; (*c*) D. J. Hodgson and E. Pedersen, *Inorg. Chem.*, 1980, **19**, 3116–3121; (*d*) J. T. Veal, D. Y. Jeter, J. C. Hempel, R. P. Eckberg, W. E. Hatfield and D. J. Hodgson, *Inorg. Chem.*, 1973, **12**, 2928–2931; (*e*) R. K. Dean, S. L. Granville, L. N. Dawe, A. Decken, K. M. Hattenhauer and C. M. Kozak, *Dalton Trans.*, 2010,

39, 548–559; (*f*) G. Novitchi, J. P. Costes, V. Ciornea, S. Shova, I. Filippova, Y. A. Simonov and A. Gulea, *Eur. J. Inorg. Chem.*, 2005, **5**, 929–937; (*g*) R. P. Scaringe, P. Singh, R. P. Eckberg, W. E. Hatfield and D. J. Hodgson, *Inorg. Chem.*, 1975, **14**, 1127–1133; (*h*) D. E. Bolster, P. Gütlich, W. E. Hatfield, S. Kremer, E. W. Müller and K. Wieghardt, *Inorg. Chem.*, 1983, **22**, 1725–1729.

15 (*a*) R. L. Carlin, *Magnetochemistry*, Springer-Verlag, Heidelberg, 1986; (*b*) R. K. Dean, S. L. Granville, L. N. Dawe, A. Decken, K. M. Hattenhauer and C. M. Kozak, *Dalton Trans.*, 2010, **39**, 548–559.

16 D. V. Konarev, S. S. Khasanov, E. I. Yudanova and R. N. Lyubovskaya, *Eur. J. Inorg. Chem.*, 2011, 816–820.

17 G. M. Sheldrick, *Acta Crystallogr., Sect. A: Fundam. Crystallogr.*, 2008, **64**, 112–122.

18 J. P. Perdew, K. Burke and M. Ernzerhof, *Phys. Rev. Lett.*, 1996, **77**, 3865–3868.

19 D. N. Laikov, *Chem. Phys. Lett.*, 2005, **416**, 116–120.

20 D. N. Laikov, *Chem. Phys. Lett.*, 1997, **281**, 151–156.